Search for the Single Production of Doubly-Charged Higgs Bosons and Constraints on its Couplings from Bhabha Scattering

The OPAL Collaboration

Abstract

A search for single production of doubly-charged Higgs bosons has been performed using 600.7 pb^{-1} of e$^+$e$^-$ collision data with $\sqrt{s} = 189$–209 GeV collected by the OPAL detector at LEP. No evidence for the existence of H$^{\pm\pm}$ is observed. Upper limits on the Yukawa coupling, h$_{ee}$, of the H$^{\pm\pm}$ to like-signed electron pairs are derived. A 95% confidence level upper limit of h$_{ee} < 0.08$ is inferred for $M(\mathrm{H}^{\pm\pm}) < 160$ GeV assuming that the sum of the branching fractions of the H$^{\pm\pm}$ to all lepton flavour combinations is 100%. Additionally, indirect constraints on h$_{ee}$ from Bhabha scattering, where the H$^{\pm\pm}$ would contribute via t-channel exchange, are derived for $M(\mathrm{H}^{\pm\pm}) < 2$ TeV. These are the first results for both a single production search and constraints from Bhabha scattering reported from LEP.

This note describes preliminary OPAL results.

1 Introduction

Some theories beyond the Standard Model predict the existence of doubly-charged Higgs bosons, $H^{\pm\pm}$, including in particular Left-Right symmetric models [1] and Higgs triplet models [2]. It has been particularly emphasized that a heavy right-handed neutrino with the see-saw mechanism to obtain light neutrinos can lead to a doubly-charged Higgs boson with a mass accessible to current and future colliders [3].

Doubly-charged Higgs bosons would decay into like-signed lepton or vector boson pairs, or to a W-boson and a singly-charged Higgs. For masses less than twice the W-boson mass, they would be expected to decay predominantly to like-signed leptons. Since the $H^{\pm\pm}$ naturally violates lepton number conservation, it can also have mixed lepton flavour decay modes. Additionally, the Yukawa coupling of the $H^{\pm\pm}$ to the charged leptons is model dependent, and is not generally determined directly by the lepton mass, so decays to all lepton flavour combinations should be considered. A review of experimental constraints on doubly-charged Higgs bosons is presented in [4]. It should be particularly noted that mixed lepton flavour decays are severely constrained by rare decay searches such as $\mu^+ \rightarrow e^+e^+e^-$ and $\mu \rightarrow e\gamma$. The pair production of doubly-charged Higgs bosons has been considered in a previous OPAL publication [5], where masses less than 98.5 GeV are excluded for doubly-charged Higgs bosons in Left-Right symmetric models.

It has been noted that doubly-charged Higgs bosons may be singly produced in $e\gamma$ collisions, including in e^+e^- collisions where the γ is obtained from radiation from the other beam particle [6, 7]. In this paper, we consider a $H^{\pm\pm}$ which couples to right-handed particles (sometimes denoted $H_R^{\pm\pm}$), but the results quoted here are insensitive to this assumption [7]. The lifetime of the $H^{\pm\pm}$ can be important, and in particular is non-negligible for $h_{\ell\ell} < 10^{-7}$; however, this Yukawa coupling is much smaller than the sensitivity of the search considered here. The diagrams for the direct production are shown in Figure 1. In this note, we use 600.7 pb^{-1} of e^+e^- collision data with $\sqrt{s} = 189$–209 GeV collected by the OPAL detector to search for the single production of doubly-charged Higgs bosons, assuming the decays $H^{\pm\pm} \rightarrow \ell^\pm\ell'^\pm$. The production cross-section depends only on h_{ee}, the Yukawa coupling of the $H^{\pm\pm}$ to like-signed electron pairs, and thus the search is sensitive to this quantity. We consider all lepton flavour combinations in the $H^{\pm\pm}$ decay (ee, $\mu\mu$, $\tau\tau$, $e\mu$, $e\tau$, $\mu\tau$), with the 100% tau-lepton branching fraction case resulting in the lowest detection efficiency.
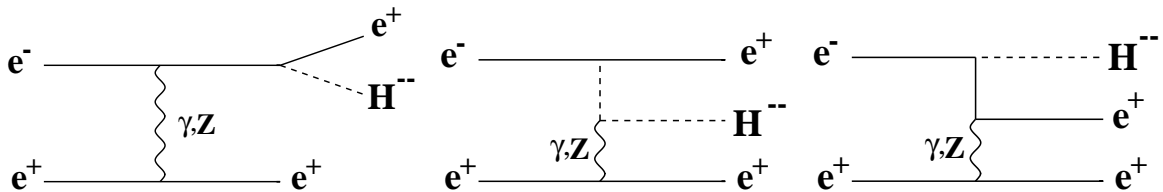

Figure 1: *Feynman diagrams contributing to the single production of* H^{--} *bosons in* e^+e^- *collisions. The three additional diagrams with "crossed"* e^+ *lines are not shown.*

A doubly-charged Higgs would also affect the Bhabha Scattering cross-section via the t-channel exchange diagram shown in Figure 2. Constraints have been derived from this process using data from lower energy colliders [4], but not previously from LEP. In addition to the direct search results, we also present constraints on the Yukawa coupling of $H^{\pm\pm}$ to electrons, h_{ee}, derived from measurements of Bhabha scattering with OPAL.
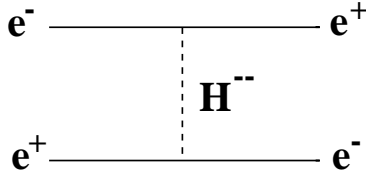
Figure 2: *Feynman diagram contributing to the process* $e^+e^- \to e^+e^-$ *due to doubly-charged Higgs t-channel exchange.*

2 OPAL Detector

The OPAL detector is described in detail in Reference [8]. It is a multipurpose apparatus with almost complete solid angle coverage. The central detector consists of two layers of silicon micro-strip detectors and a system of gas-filled tracking chambers in a 0.435 T solenoidal magnetic field which is parallel to the beam axis. A lead-glass electromagnetic calorimeter with a presampler surround the central detector. In combination with the forward calorimeters, the forward scintillating-tile counters, and the silicon-tungsten luminometer, a geometrical acceptance is provided down to 25 mrad from the beam direction. The silicon-tungsten luminometer measures the integrated luminosity using small-angle Bhabha scattering events. The magnet return yoke is instrumented for hadron calorimetry, and is surrounded by several layers of muon chambers.

3 Direct Search

3.1 Event Simulation and Data Sample

A data set of 600.7 pb^{-1} with $\sqrt{s} = 189$–209 GeV is analyzed. The data samples are summarized in Table 1.

E_{cm} (GeV)	$\langle E_{\text{cm}} \rangle$ (GeV)	$\int \mathcal{L}$ (pb^{-1})
$188 - 190$	188.6	175.0
$190 - 194$	191.6	28.9
$194 - 198$	195.5	74.8
$198 - 201$	199.5	78.1
$201 - 203$	201.7	38.2
$203 - 206$	205.0	79.4
$206 - 210$	206.6	126.1
$188 - 210$	197.7	600.7

Table 1: *Data samples used in the direct search analysis.*

The process $e^+e^- \to e^\mp e^\mp H^{\pm\pm}$ is simulated with the PYTHIA [9] event generator. In the simulation, the Equivalent Photon Approximation (EPA) is used to give an effective flux of photons inside the electrons. The upper limit of the virtuality Q^2 is given by the scale of the hard scattering process. Finally, the process $e^\pm\gamma \to e^\mp H^{\pm\pm}$ is simulated using the calculations from [6]. This approximation does not strictly correspond to the full set of diagrams in Figure 1, and it was noted in [6] that using EPA does not accurately represent the full differential cross-section for this process. The particularly problematic region is where the "third lepton" ($e^\mp$) is scattered at low angle, in which case the electron mass and interference among the 3 diagrams is

important. By requiring a visible "third lepton" ($e^{\mp}$) in the selection, these regions are largely avoided. We have validated the method used here by comparison of the PYTHIA results with a direct calculation of the process $e^+e^- \rightarrow e^{\mp}e^{\mp}H^{\pm\pm}$ in the restricted angular range considered in this note, finding $\mathcal{O}(20\%)$ agreement in the production cross-sections [10]. Separate samples are simulated with the 6 different decay modes (ee, $\mu\mu$, $\tau\tau$, eμ, eτ, $\mu\tau$). Samples of 500 events each were generated for each of the centre-of-mass energies listed in Table 1 for $H^{\pm\pm}$ masses in 5 GeV steps from 90–160 GeV. Larger masses are not currently considered in the direct search because of the model dependence of the $H^{\pm\pm} \rightarrow W^{\pm}W^{\pm}$ branching fraction.

The dominant Standard Model backgrounds in this analysis are from the four-fermion processes $e^+e^- \rightarrow \ell^+\ell^-\ell'^+\ell'^-$, including events from the so-called "multi-peripheral" diagrams $e^+e^- \rightarrow e^+e^-\gamma^{(*)}\gamma^{(*)} \rightarrow e^+e^-\ell^+\ell^-$. The processes $e^+e^- \rightarrow \ell^+\ell^-\ell'^+\ell'^-$, and also all hadronic and semi-leptonic four-fermion processes, with no electrons in the final state are simulated with the KORALW event generator [11] and cross-checked with grc4f [12]. KORALW uses the same matrix elements as grc4f. The non-multi-peripheral part of the process $e^+e^- \rightarrow e^+e^-\ell^+\ell^-$ (including $\ell = e$) is simulated with grc4f. The multi-peripheral diagrams are simulated with the dedicated two-photon event generators Vermaseren [13] for $e^+e^- \rightarrow e^+e^-\gamma^{(*)}\gamma^{(*)} \rightarrow e^+e^-e^+e^-$ and BDK [14] for $e^+e^- \rightarrow e^+e^-\gamma^{(*)}\gamma^{(*)} \rightarrow e^+e^-\mu^+\mu^-$ and $e^+e^- \rightarrow e^+e^-\gamma^{(*)}\gamma^{(*)} \rightarrow e^+e^-\tau^+\tau^-$. Since this prescription ignores possible interference between multi-peripheral and non-multi-peripheral diagrams, the background is checked using $e^+e^- \rightarrow e^+e^-\ell^+\ell^-$ samples generated with grc4f2.2 which contain all diagrams and the interference among them.

The backgrounds from other processes are also considered in the analysis. Lepton pairs were simulated using the KK2f [15] generator for $\tau^+\tau^-(\gamma)$ and $\mu^+\mu^-(\gamma)$ events and NUNUGPV [16] for $\nu\bar{\nu}\gamma(\gamma)$. Bhabha scattering was simulated with BHWIDE [17] (when both the electron and positron scatter at least $12.5°$ from the beam axis) and TEEGG [18] (for the remaining phase space). RADCOR [19] is used to simulate multi-photon events from QED processes. Multihadronic events, $q\bar{q}(\gamma)$, were simulated using KK2f [15]. The purely photonic final states make a negligible contribution to the background. The Monte Carlo generators PHOJET [20] (for $Q^2 < 4.5$ GeV^2) and HERWIG [21] (for $Q^2 \geq 4.5$ GeV^2)[1] are used to simulate hadronic events from two-photon processes.

Generated signal and background events were processed through the full simulation of the OPAL detector [22] and the same event analysis chain was applied to the simulated events as to the data.

3.2 Analysis

Events are reconstructed from charged particle tracks and energy deposits (clusters) in the electromagnetic and hadron calorimeters. Tracks and clusters are defined to be of "good" quality using the requirements of [23]. After the event reconstruction, double-counting of energy between tracks and calorimeter clusters is corrected by reducing the calorimeter cluster energy by the expected energy deposition from associated charged tracks [23], including particle identification information.

The signal final states considered in this note consist of three leptons visible in the detector, two of which have the same sign and originate from the decay of a doubly-charged Higgs. The remaining electron or positron is usually close to the beam direction and escapes detection. Leptons are identified as low multiplicity jets. No explicit electron or muon identification is applied, since it is found that the jet-based analysis technique retains high efficiency while reducing the background to an acceptable level. The final background is dominated by Standard Model processes containing four charged leptons. The same analysis is used to search for all 6

---

[1]Q^2 is the negative squared four-momentum transfer.

possible lepton flavour combinations, and the results are valid for all leptonic decay modes of the $H^{\pm\pm}$. The analysis cuts listed below are applied.

(1) The preselection requires low multiplicity events [25] that pass the $W^+W^- \to \ell\nu\ell\nu$ preselection requirements [26]. The events are additionally required to have at least 2 charged tracks. Tracks and clusters are formed into jets using a cone algorithm with a half-angle of 20 degrees [24], and it is required that there are at least 2 jets with polar angles satisfying $|\cos\theta| < 0.95$, and which are not precisely back-to-back (within $5°$). Finally, the sum of the energies of the 3 most energetic jets reconstructed in the event (where the third jet energy is defined to be zero if there are only 2 jets) must be greater than 20% of $\sqrt{s}$.

(2) The analysis requires at least 3 jets in the event, and additional jets are not used in the analysis. Ordering the jet energies by their magnitude ($E_{\mathrm{jet1}} > E_{\mathrm{jet2}} > E_{\mathrm{jet3}}$), the following requirements are made:

    a) $E_{\mathrm{jet1}} > 0.1\sqrt{s}$;

    b) $E_{\mathrm{jet2}} > 0.05\sqrt{s}$;

    c) $E_{\mathrm{jet3}} > 0.025\sqrt{s}$ or it must contain at least one charged track;

    d) $E_{\mathrm{jet1}} < 0.995 E_{\mathrm{beam}}$;

    e) $E_{\mathrm{jet1}} + E_{\mathrm{jet2}} + E_{\mathrm{jet3}} < 0.95\sqrt{s}$.

(3) The estimates of the energies of the jets are improved by assuming that the measured jet direction is the same as the initial lepton direction for each of the 3 reconstructed jets, and further assuming that the missing electron or positron is recoiling along the beam axis. Using energy and momentum conservation to give four constraint equations, the four jet energies can be inferred (the lepton masses are neglected). Using this improved determination of the jet energies, the three possible di-jet masses of the observed jets are calculated, and the two jets having the largest di-jet mass are considered as the $H^{\pm\pm}$ candidate jets with a "reconstructed Higgs mass" M_{rec}. Typical mass resolutions are about 1 GeV for ee and $\mu\mu$ modes, and about 4 GeV for $\tau\tau$ decays. Since this search concentrates on the region above the mass limit from pair creation and below twice the W-boson mass, it is further required that M_{rec} satisfy 80 GeV $< M_{\mathrm{rec}} <$ 180 GeV.

(4) Bhabha scattering is rejected by requiring that the acollinearity angle, ϕ_{acol}, satisfy $\phi_{\mathrm{acol}} > 20°$. The angle ϕ_{acol} is defined to be $180°$ minus the opening angle of the two most energetic jets.

(5) The polar angle of each jet associated to the $H^{\pm\pm}$ must satisfy $|\cos\theta| < 0.8$. The $H^{\pm\pm}$ candidate jet polar angles are plotted in Figures 3(a) and (b) after cuts (1)–(4) have been applied.

(6) Each jet associated to the $H^{\pm\pm}$ must have either 1 or 3 charged tracks. The number of charged tracks is plotted in Figure 3(c) after cuts (1)–(5) have been applied.

(7) Defining the sum of the track charges within each jet as the "jet charge," the product of the charges of the two jets associated with the $H^{\pm\pm}$ must be equal to $+1$. The product of the reconstructed charges of the two $H^{\pm\pm}$ candidate jets is plotted in Figure 3(d) after cuts (1)–(6) have been applied.

The results are summarized in Table 2. The numbers of observed and expected events agree well after each cut in the analysis.

Cut	Data	Total Bkg.	$\ell^+\ell^-$	4-ℓ	'$\gamma\gamma$' ee$\ell\ell$	q$\bar{\text{q}}$	'$\gamma\gamma$' eeqq	130 GeV H$^{\pm\pm}$ h$_{ee}$ = 0.1		
								ee	$\mu\mu$	$\tau\tau$
(1)	59995	58878.9	21708.8	1757.2	29172.7	373.8	5866.4	82.7	82.0	74.9
(2)	11299	11267.6	2892.7	309.3	7086.3	151.3	828.0	65.3	56.6	63.8
(3)	4002	3876.2	2372.5	158.0	1179.3	92.0	74.4	61.9	53.9	53.9
(4)	2652	2522.5	1432.6	123.6	856.4	66.1	43.8	55.5	50.0	51.2
(5)	520	517.8	415.5	41.1	49.0	11.8	0.4	37.8	37.2	34.2
(6)	345	336.4	252.4	32.4	46.6	4.9	0.1	36.5	36.5	30.5
(7)	26	21.2	3.8	5.0	11.9	0.5	0.1	36.0	36.1	29.3
		±1.4	±0.5	±0.4	±1.3	±0.1	±0.0	±1.5	±1.5	±1.6

Table 2: *The remaining numbers of events in the data after each cut, and the number expected from Standard Model background sources. Also shown are the numbers of expected signal events for a 130 GeV doubly-charged higgs normalized to a cross-section corresponding to* h$_{ee}$ = 0.1 *assuming ee, $\mu\mu$ or $\tau\tau$ decays. The errors due to Monte Carlo statistics are also listed for events surviving the full analysis.*

3.3 Systematic Errors

The largest background in the selection is from 4-charged lepton production, particularly from multi-peripheral "two-photon" processes. Of concern is the fact that, in our standard Monte Carlo background samples available at all centre-of-mass energies, the multi-peripheral diagrams are treated with specialized event generators which neglect interference with non-multi-peripheral diagrams. Special samples of the full set of $e^+e^- \rightarrow e^+e^-\ell^+\ell^-$ diagrams, including interference, were prepared using grc4fv2.2 [12] at $\sqrt{s}$ = 206 GeV to study this effect. The background using the full set of $e^+e^-\ell^+\ell^-$ diagrams including interference is $(26.6\pm6.6)\%$ lower than our standard set of Monte Carlo generators. While this new method of evaluating the $e^+e^-\ell^+\ell^-$ is, in principle, better than our standard method, it has not yet been sufficiently well studied to warrant a correction of the central value of the background expectation, nor to claim that the difference is in fact due to interference effects; instead, a systematic error of 27% on the background level is assigned from this check.

Monte Carlo modelling of the variables used in the selection cuts can also induce systematic effects. The possible level of mismodelling is assessed by comparing data and background Monte Carlo for each variable at a loose selection level where the contribution from a signal would be negligible. Differences between the data and background Monte Carlo simulation are used to define a possible shift in each variable, and then the systematic errors are evaluated by varying the cuts by these shifts. Both the final expected background and signal efficiencies are recalculated with these shifted cuts, and the full differences with the nominal values are assigned as systematic errors.

The possible mismodelling of the jet charge determination in the Monte Carlo, used in cut (7) in Section 3.2 to reject a significant fraction of the background, has not yet been fully evaluated. Currently, the full magnitude of the fraction of tracks estimated in the Monte Carlo to have a mismeasured charge is taken as a systematic error. The systematic errors on the background and signal efficiencies are evaluated by randomly changing the sign of the charge of 1% of the the tracks in the Monte Carlo samples. The full differences between the new background and efficiencies and the nominal ones are taken as systematic errors.

The systematic errors are summarized in Table 3. Additional systematic errors, such as on the integrated luminosity, are negligible.

Quantity	Variation	Δ Bkg (%)	Δ Sig (%)
Jet $\cos\theta$	$(\pm 0.5°)$	5	1
Jet Energy	$\pm 1\%$	1	1
$\phi_{\rm acol}$	$\pm 0.5°$	1	1
Charge Misidentification	1%	26	2
Bkg Modelling	(see text)	27	–
Monte Carlo Statistics	–	7	5
Quadratic Sum		38	6

Table 3: *Systematic errors on signal and background.*

3.4   Direct Search Results

The $H^{\pm\pm}$ candidate reconstructed masses, $M_{\rm rec}$, using the "angle-based" kinematic reconstruction described in item (3) in Section 3.2, are shown in Figure 4. Additionally, as a cross-check to ensure that no di-jet mass peak present after event reconstruction is reduced by the angle-based method, the largest di-jet mass calculated from only the track and cluster information (Section 3.2) is plotted in Figure 5. Note that the jet combination with the largest di-jet mass need not be the same combination that gives the largest $M_{\rm rec}$ using the angle-based reconstruction technique, and not all selected events are actually contained in the range plotted in this figure. The mass distributions are shown both for events passing all cuts except the like-signed charge requirement, and also with that cut applied. No peaks are observed in the data.

Limits are set on the $H^{\pm\pm}$ Yukawa coupling $h_{\rm ee}$, assuming that the sum of the branching fractions of the $H^{\pm\pm}$ to all lepton flavour combinations is 100%. The efficiency for an arbitrary Higgs mass is determined by linear interpolation between the simulated signal Monte Carlo samples. The limits are calculated using the program described in [27], which incorporates the systematic errors into the limits using a numerical convolution technique. For the purpose of extracting the limits, a ± 10 GeV "sliding mass window" is used to count events in the data and to evaluate the background expectation consistent with each Higgs test mass in 1 GeV steps. A small efficiency correction due to this window is applied.

The limits on $h_{\rm ee}$ are calculated using the efficiencies determined from the PYTHIA Monte Carlo samples and the production cross-sections are determined in a consistent manner using PYTHIA (see discussion in Section 3.1). No additional systematic error is assigned for theoretical uncertainties. The 95% confidence level limits on $h_{\rm ee}$ are shown in Figure 6 for different leptonic decay modes. For the worst case of 100% decays to $\tau\tau$, an upper limit of $h_{\rm ee} < 0.08$ is inferred for $M(H^{\pm\pm}) < 160$ GeV, which is valid for all possible lepton flavour combinations in the decays. For masses above 160 GeV, the decays of the $H^{\pm\pm}$ into W pairs may become non-negligible depending on the specific model used and limits are not quoted.

4   Indirect Search

Doubly-charged Higgs bosons would contribute to Bhabha scattering via t-channel exchange as shown in Figure 2. The Born level differential cross-section for Bhabha scattering including the exchange of a doubly-charged Higgs boson with right-handed couplings has been calculated in [4]. At high masses, $M(H^{\pm\pm}) \gg \sqrt{s}$, the cross-section is identical to that derived for four-fermion contact interactions [28] with $\eta_{\rm RR} = 1$, $\eta_{\rm LL} = \eta_{\rm LR} = 0$, with the replacement of g/Λ by $h_{\rm ee}/M(H^{\pm\pm})$ where $h_{\rm ee}$ is the Higgs coupling to electrons[2]. At values of $M(H^{\pm\pm})$ comparable

---
[2]In [4] $h_{\rm ee}$ is denoted $g_{\rm ee}$.

to the centre-of-mass energy, this correspondence is modified by the inclusion of a propagator term. For comparison with the experimental data, QED radiative corrections to $\mathcal{O}(\alpha)$ have been applied to the Born level terms for doubly-charged Higgs exchange and interference with Standard Model processes given in [4] using the program MIBA [29]. The BHWIDE [17] program was used to calculate the Standard Model contribution to the differential cross-section. The theoretical predictions are calculated using the same acceptance cuts as have been applied to the data.

This analysis uses published OPAL measurements of the differential cross-section for $\mathrm{e^+e^-} \to \mathrm{e^+e^-}$ at centre-of-mass energies of 183 GeV [30] and 189 GeV [31], together with preliminary measurements at 192 GeV, 196 GeV, 200 GeV and 202 GeV [32] and at energies between 203 GeV and 209 GeV [33]. The data between 203 GeV and 209 GeV are grouped into two sets with mean energies of approximately 205 GeV and 207 GeV. The total integrated luminosity of the data amounts to approximately 680 pb^{-1}. These measurements cover the range $|\cos\theta| < 0.9$, in nine bins of $\cos\theta$, and correspond to $\theta_{\mathrm{acol}} < 10°$ where θ_{acol} is the acollinearity angle between electron and positron. It was verified that the effect of doubly-charged Higgs exchange on the low-angle Bhabha Scattering cross-section has a negligible effect on the luminosity determination.

The measured differential cross-sections have been fitted with the theoretical prediction using a χ^2 fit. The fit was performed for fixed values of the doubly-charged Higgs mass between 20 GeV and 2000 GeV, allowing the square of the coupling, $\mathrm{h}_{\mathrm{ee}}^2$, to vary. Both positive and negative values of $\mathrm{h}_{\mathrm{ee}}^2$ were allowed in the fit, although only $\mathrm{h}_{\mathrm{ee}}^2 > 0$ is physically meaningful, in order to allow for the case where the data fluctuate in the opposite direction to that expected for doubly-charged Higgs exchange. Experimental and theoretical systematic errors and their correlations were treated as discussed in [34]. The fitted values of $\mathrm{h}_{\mathrm{ee}}^2$ are consistent with zero for all masses, indicating that the data are consistent with the Standard Model prediction. For example, for a mass of 130 GeV the fitted value of $\mathrm{h}_{\mathrm{ee}}^2$ is –0.004±0.009, and the fit has a χ^2 of 80.7 for 71 degrees of freedom. Figure 7 shows the ratio of the measurements to the Standard Model prediction at 207 GeV, together with the results of the fit. 95% confidence level limits on the coupling as a function of mass were derived by integrating the likelihood function derived from χ^2 over the region $\mathrm{h}_{\mathrm{ee}}^2 > 0$, and are shown in Figure 8. The limits are considerably more stringent than those derived from PEP and PETRA data [4]. Figure 6(d) shows the limits from the indirect search together with those from the direct search. The indirect limits are less restrictive than those from the direct search at low masses, but extend to much higher masses.

5   Conclusion

A direct search for the single production of doubly-charged Higgs bosons has been performed. No evidence for the existence of $\mathrm{H^{\pm\pm}}$ is observed. Upper limits on the Higgs Yukawa coupling to like-signed electron pairs, h_{ee}, are determined. A 95% confidence level upper limit of $\mathrm{h}_{\mathrm{ee}} < 0.08$ is inferred for $M(\mathrm{H^{\pm\pm}}) < 160$ GeV assuming that the sum of the branching fractions of the $\mathrm{H^{\pm\pm}}$ to all lepton flavour combinations is 100%. Additionally, indirect constraints on h_{ee} from Bhabha scattering where the $\mathrm{H^{\pm\pm}}$ would contribute via t-channel exchange are derived for $M(\mathrm{H^{\pm\pm}}) < 2$ TeV. These are the first results on both the single production search and constraints from Bhabha scattering reported from LEP.

References

[1] J.C. Pati and A. Salam, Phys. Rev. **D10** (1974) 275;
R.N. Mohapatra and J.C. Pati, Phys. Rev. **D11** (1975) 566, 2558;
G. Senjanovic and R.N. Mohapatra, Phys. Rev. **D12** (1975) 1502;
R.N. Mohapatra and R.E. Marshak, Phys. Lett. **B91** (1980) 222;
R.N. Mohapatra and D. Sidhu, Phys. Rev. Lett. **38** (1977) 667.

[2] G.B. Gelmini and M. Roncadelli, Phys. Lett. **B99** (1981) 411.

[3] C. S. Aulakh, A. Melfo and G. Senjanovic, Phys. Rev. **D57** (1998) 4174;
Z. Chacko and R. N. Mohapatra, Phys. Rev. **D58** (1998) 15003;
B. Dutta and R. N. Mohapatra, Phys. Rev. **D59** (1999) 15018.

[4] M.L. Swartz, Phys. Rev. **D40** (1989) 1521.

[5] OPAL Collab., G. Abbiendi *et al.* Phys. Lett. **B526** (2002) 221.

[6] G. Barenboim, K. Huitu, J. Maalampi and M. Raidal, Phys. Lett. **B394** (1997) 132.

[7] S. Godfrey, P. Kalyniak and N. Romanenko, Phys. Rev. **D65** (2002) 33009.

[8] OPAL Collab., K. Ahmet *et al.*, Nucl. Instr. Meth. **A305** (1991) 275;
S. Anderson *et al.*, Nucl. Instr. Meth. **A403** (1998) 326;
B.E. Anderson *et al.*, IEEE Trans. on Nucl. Science **41** (1994) 845;
G. Aguillion *et al.*, Nucl. Instr. Meth. **A417** (1998) 266.

[9] T. Sjöstrand, Comp. Phys. Comm. **39** (1986) 347;
T. Sjöstrand, PYTHIA 5.7 and JETSET 7.4 Manual, CERN-TH 7112/93.

[10] Personal communication, S. Godfrey and P. Kalyniak.

[11] Program KORALW V1.33, M. Skrzypek *et al.*, Comp. Phys. Comm. **94** (1996) 216;
M. Skrzypek *et al.*, Phys. Lett. **B372** (1996) 286.

[12] J. Fujimoto *et al.*, Comp. Phys. Comm. **100** (1997) 128.

[13] J.A.M. Vermaseren, Nucl. Phys. **B229** (1983) 347.

[14] F.A. Berends, P.H. Daverveldt and R. Kleiss, Nucl. Phys. **B253** (1985) 421; Comp. Phys. Comm. **40** (1986) 271, 285, 309.

[15] S. Jadach, B.F.L. Ward and Z. Was, Phys. Lett. **B449** (1999) 97.

[16] G. Montagna, M. Moretti, O. Nicrosini and F. Piccinini, Nucl. Phys. **B541** (1999) 31.

[17] S. Jadach, W. Płaczek and B.F.L. Ward, Phys. Lett. **B390** (1997) 298.

[18] D. Karlen, Nucl. Phys. **B289** (1987) 23.

[19] F.A. Berends and R. Kleiss, Nucl.Phys. **B186** (1981) 22.

[20] E. Boudinov *et al.*, 'γγ Event Generators', hep-ph/9512371, Dec. 1995, and in 'Physics at LEP2', eds. G. Altarelli, T. Sjöstrand and F. Zwirner, CERN 96-01, vol.2 (1996) 187.

[21] G. Marchesini *et al.*, Comp. Phys. Comm. **67** (1992) 465.

[22] J. Allison *et al.*, Nucl. Instr. Meth. **A317** (1992) 47.

[23] OPAL Collab., K. Ackerstaff *et al.*, Eur. Phys. J. **C2** (1998) 213.

[24] OPAL Collab., R. Akers *et al.* Z.Phys.**C63** (1994) 197.

[25] OPAL Collab., G. Alexander *et al.* Z.Phys. **C52** (1991) 175.

[26] OPAL Collab., G. Abbiendi *et al.* Phys. Lett. **B493** (2000) 249.

[27] T. Junk, Nucl.Instrum.Meth. **A434** (1999) 435.

[28] E. Eichten, K. Lane and M. Peskin, Phys. Rev. Lett. **50** (1983) 811.

[29] M. Martinez and R. Miquel, Z.Phys. **C53** (1992) 115.

[30] OPAL Collab., G. Abbiendi et al., Eur. Phys. J. **C6** (1999) 1.

[31] OPAL Collab., G. Abbiendi et al., Eur. Phys. J. **C13** (2000) 553.

[32] OPAL Collab., *Tests of the Standard Model and Constraints on New Physics from Measurements of Fermion-pair Production at 192–202 GeV at LEP*, OPAL Physics Note PN424 (March 2000).

[33] OPAL Collab., *Measurement of Standard Model Processes in* e^+e^- *Collisions at* $\sqrt{s} \sim 203$–*209 GeV*, OPAL Physics Note PN469 (February 2001).

[34] OPAL Collab., *Limits on Low Scale Quantum Gravity in Extra Spatial Dimensions from Measurements of* $e^+e^- \rightarrow e^+e^-$ *at LEP*, OPAL Physics Note PN471 (February 2001).
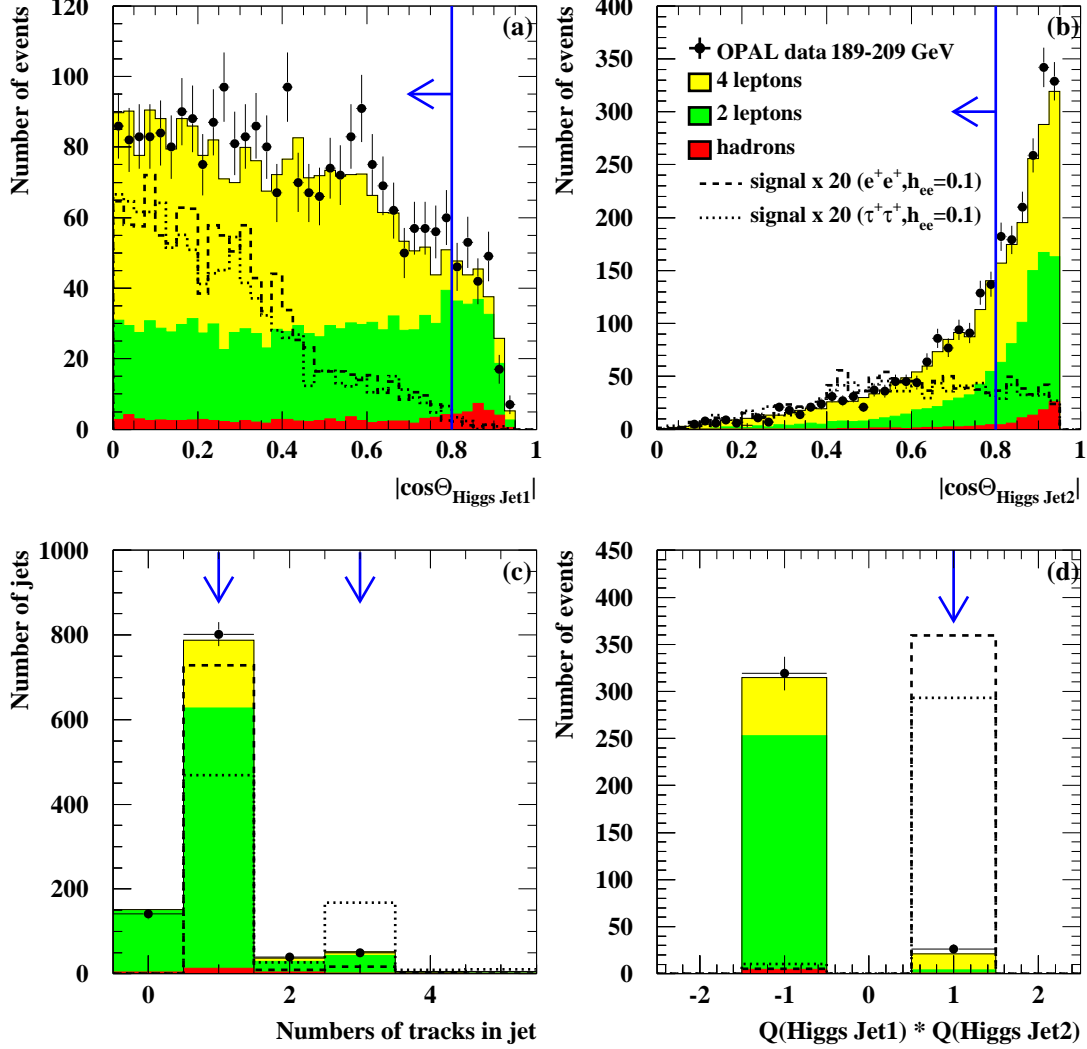
Figure 3: Examples of some of the quantities used in the selection shown immediately before the corresponding cut is applied (see Section 3.2). The absolute value of the cosine of the polar angles of the highest and second highest energy Higgs candidate jets are shown in (a) and (b), the number of charged tracks in the two $H^{\pm\pm}$ candidate jets in (c), and the product of the reconstructed charges of the two $H^{\pm\pm}$ candidate jets in (d). The points indicate the OPAL data and the shaded regions indicate the background expectation. Note that "hadrons" includes both $q\bar{q}(\gamma)$ and hadronic events from all 4-fermion processes. Two example signal expectations for a 130 GeV doubly-charged Higgs are also shown normalized to a cross-section corresponding to $h_{ee} = 0.1$, assuming either a 100% $H^{\pm\pm} \rightarrow ee$ branching ratio (dashed line) or a 100% $H^{\pm\pm} \rightarrow \tau\tau$ branching ratio (dotted line). The cut requirements are indicated by the arrows.
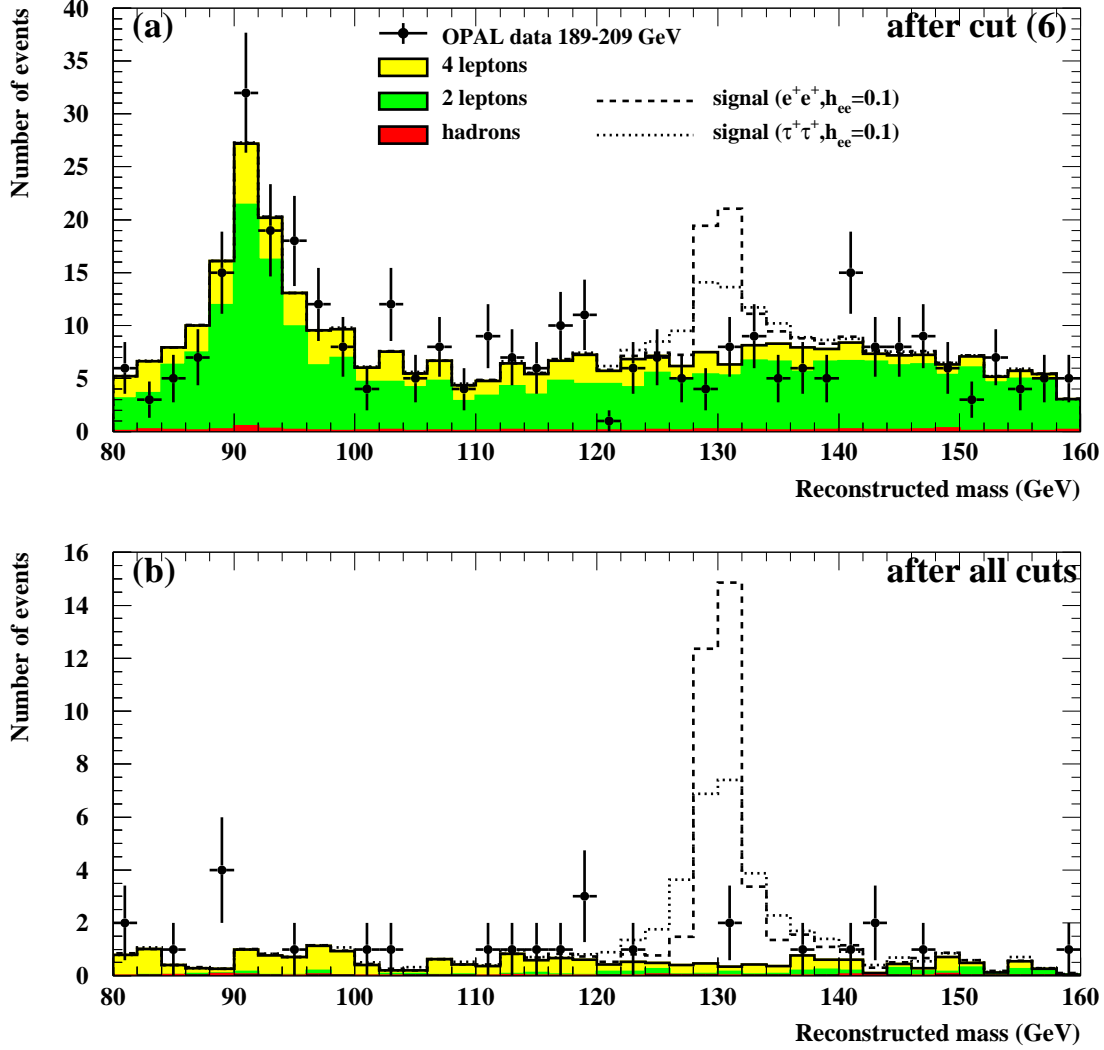
OPAL preliminary

Figure 4: The reconstructed $H^{\pm\pm}$ mass using the jet angles, as discussed in the text. The results are shown both without and with the like-signed jet requirement (cut 7) in (a) and (b), respectively. The points indicate the OPAL data and the shaded regions indicate the background expectation. Note that "hadrons" includes both $q\bar{q}(\gamma)$ and hadronic events from all 4-fermion processes. Two example signal expectations for a 130 GeV doubly-charged Higgs are also shown normalized to a cross-section corresponding to $h_{ee} = 0.1$, assuming either a 100% $H^{\pm\pm} \to ee$ branching ratio (dashed line) or a 100% $H^{\pm\pm} \to \tau\tau$ branching ratio (dotted line).
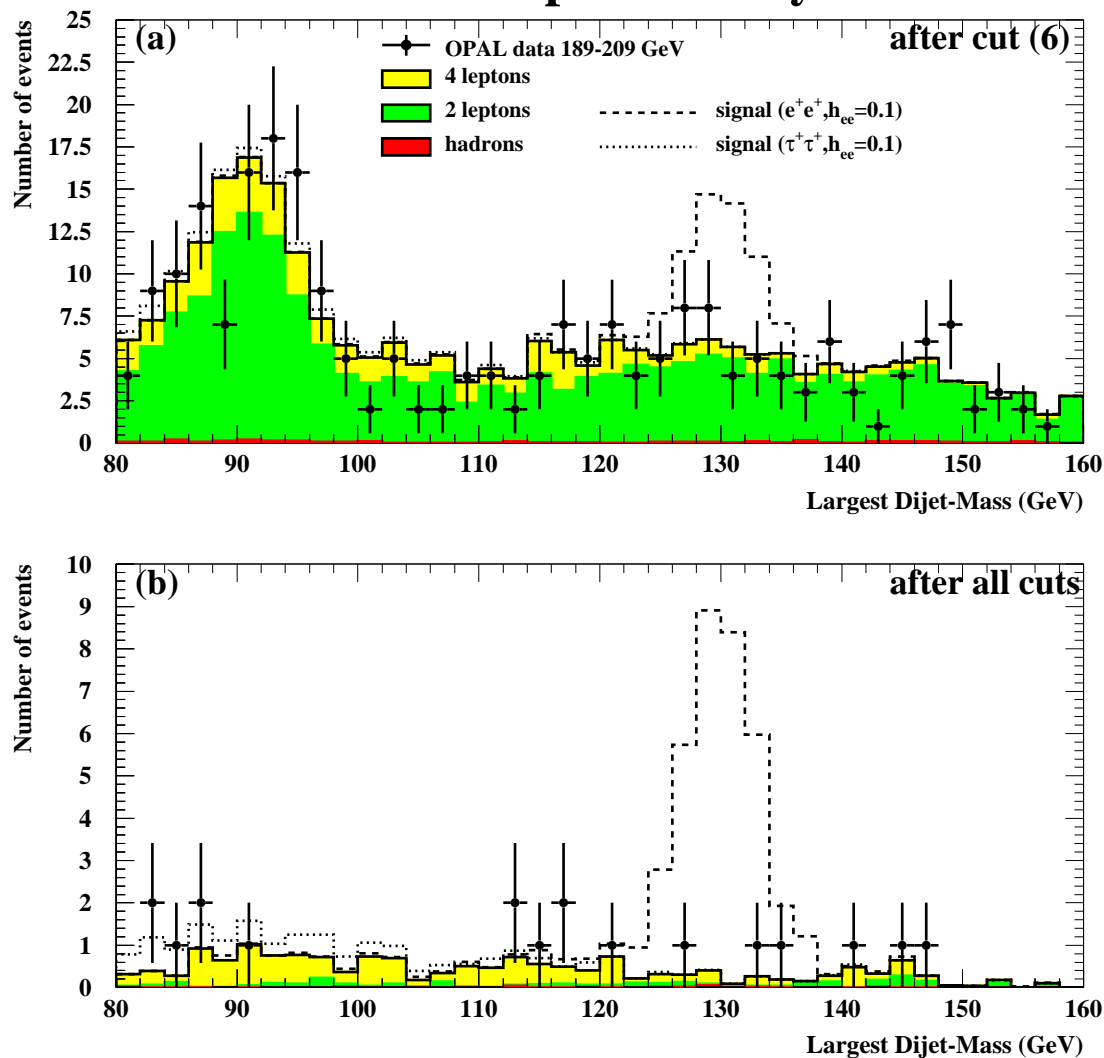
11

OPAL preliminary

Figure 5: The largest di-jet mass in the event calculated using only tracking and calorimeter information (*i.e.* not using the angle-based reconstruction discussed in the text). The results are shown both without and with the like-signed jet requirement (cut 7) in (a) and (b), respectively. The points indicate the OPAL data and the shaded regions indicate the background expectation. Note that "hadrons" includes both $q\bar{q}(\gamma)$ and hadronic events from all 4-fermion processes. Two example signal expectations for a 130 GeV doubly-charged Higgs are also shown normalized to a cross-section corresponding to $h_{ee} = 0.1$, assuming either a 100% $H^{\pm\pm} \to ee$ branching ratio (dashed line) or a 100% $H^{\pm\pm} \to \tau\tau$ branching ratio (dotted line). Note that there is no peak in the $H^{\pm\pm} \to \tau\tau$ signal sample due to the missing neutrinos from the tau-lepton decays.
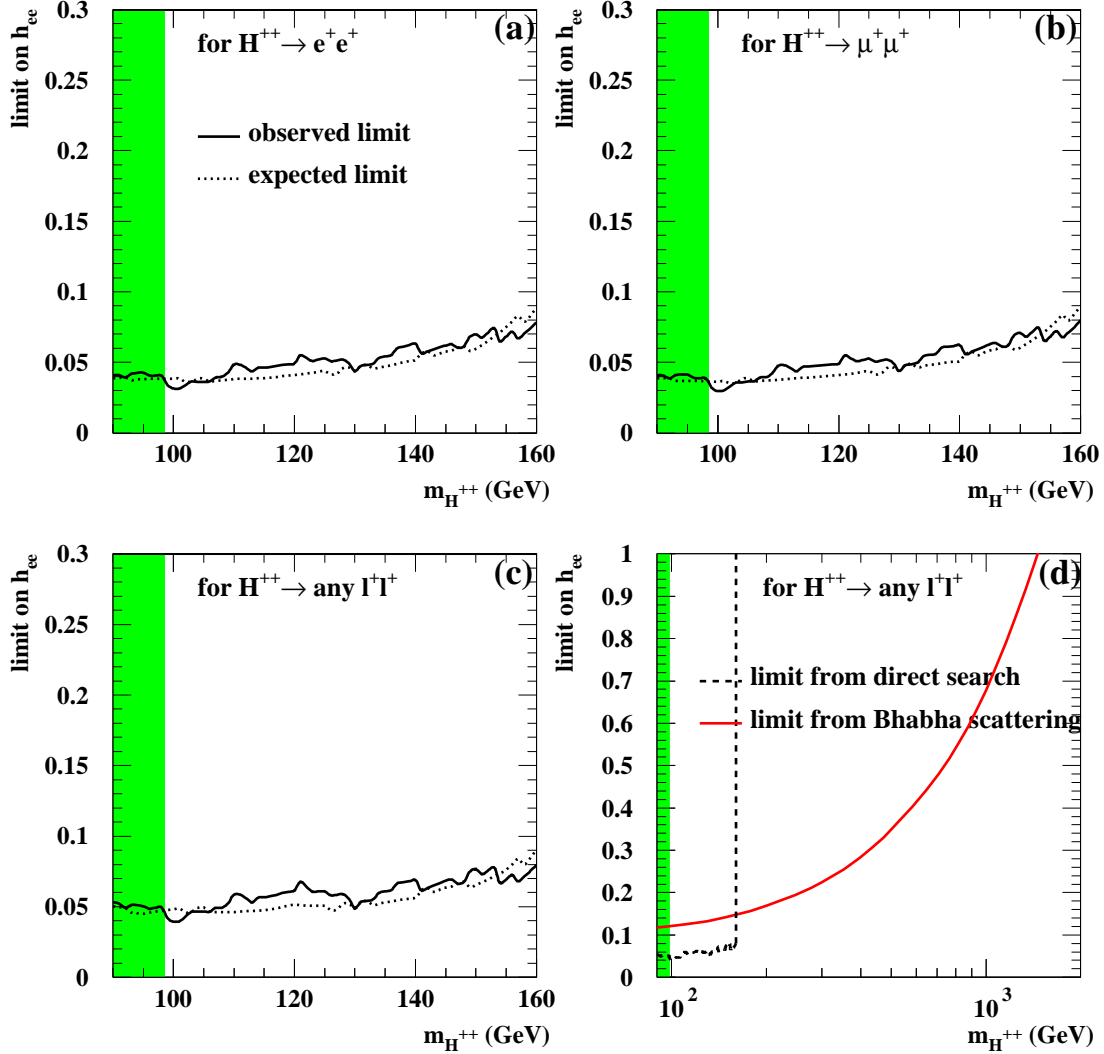
Figure 6: Limits at the 95% confidence level on the Yukawa coupling h_{ee} assuming a 100% branching fraction of the $H^{\pm\pm}$ to (a) ee, (b) $\mu\mu$ and (c) $\tau\tau$. In (b) and (c), the limits should be regarded as valid in the large branching fraction limit, since non-zero h_{ee} implies a non-zero electron branching fraction. Since the ee and $\mu\mu$ efficiencies and mass resolutions are extremely similar, plots (a) and (b) are almost identical. The median expected limits assuming only Standard Model processes are shown by the dashed lines, while the actual limits inferred from the data are shown by the solid lines. Since the $\tau\tau$ efficiency is lower than any other lepton flavour combination, plot (c) is valid for all 6 possible lepton flavour combinations (ee, eμ, eτ, $\mu\mu$, $\mu\tau$ and $\tau\tau$). The shaded regions for masses below 98.5 GeV are excluded by the OPAL pair production search [5]. In (d), the limit on h_{ee} obtained from Bhabha Scattering described in Section 4 is also shown.

OPAL preliminary

$e^+e^- \rightarrow e^+e^-$

$\sqrt{s} = 207$ GeV

— best fit to all data

······· 95% c.l. from fit to all data

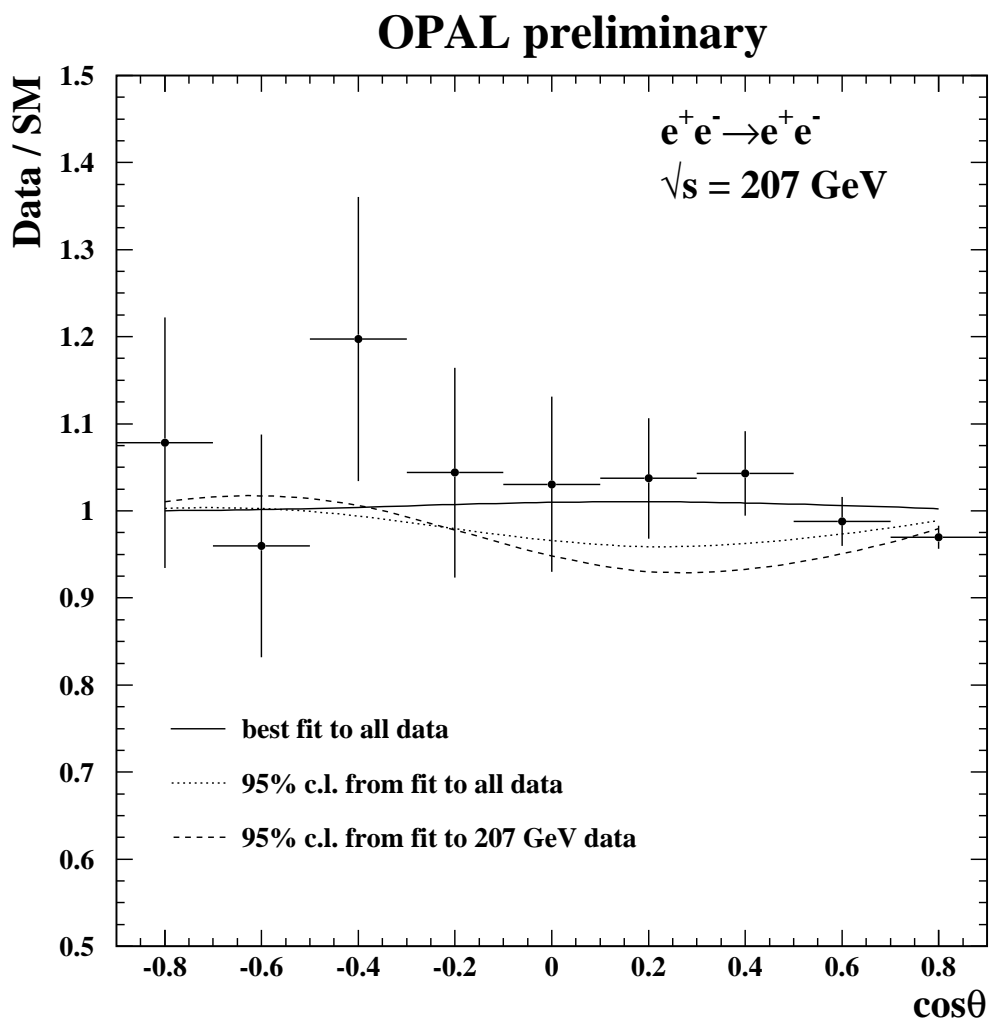----- 95% c.l. from fit to 207 GeV data

Figure 7: Ratio of the measured differential cross-section for $e^+e^- \rightarrow e^+e^-$ to the Standard Model prediction at 207 GeV. The points show the OPAL data, while the curves show theoretical predictions for a doubly-charged Higgs mass of 130 GeV. The solid curve corresponds to the best fit to all data, the dotted curve corresponds to a coupling equal to the 95% confidence level limit. For comparison, the dashed curve shows the theoretical expectation for a coupling equal to the 95% confidence level limit obtained from fitting 207 GeV data alone.
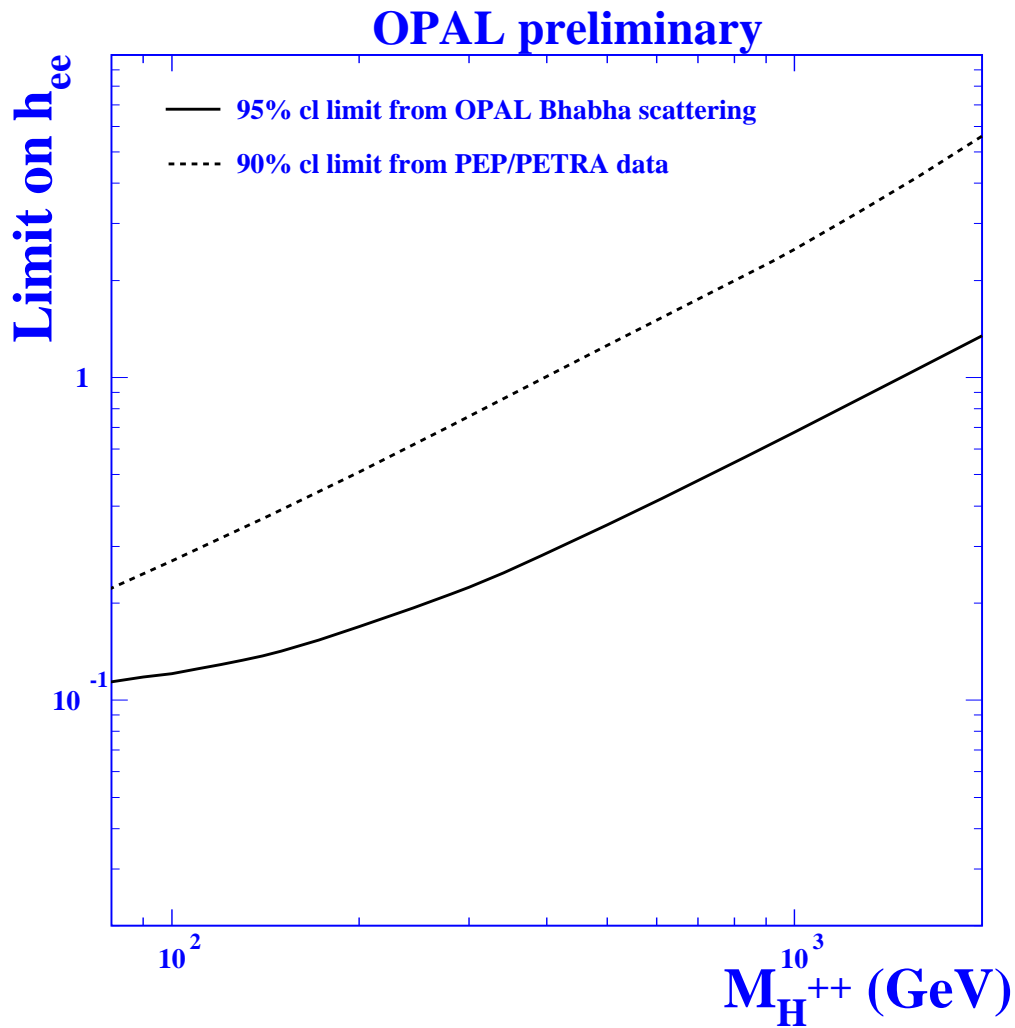
Figure 8: Limits at the 95% confidence level on the Yukawa coupling h_{ee} as a function of $M(H^{\pm\pm})$ derived from Bhabha scattering data (solid line). Limits derived from PEP and PE-TRA data [4] are shown, as a dashed line, for comparison; these are at 90% confidence level.